

Article

Interactions of Ruddlesden-Popper Phases and Migration-Induced Field-Stabilized Polar Phase in Strontium Titanate

Christian Ludt^{1,†}, Elena Ovchinnikova² , Anton Kulikov³ , Dmitri Novikov⁴, Sibylle Gemming⁵ , Dirk C. Meyer¹ and Matthias Zschornak^{1,5,*},[†]

- ¹ Institute of Experimental Physics, Technische Universität Bergakademie Freiberg, Leipziger Str. 23, 09599 Freiberg, Germany; christian.ludt@physik.tu-freiberg.de (C.L.); dirk-carl.meyer@physik.tu-freiberg.de (D.C.M.)
- ² Physics Department, Moscow State University, 119991 Moscow, Russia; ovtchin@gmail.com
- ³ A.V. Shubnikov Institute of Crystallography, FSRC “Crystallography and Photonics” RAS, Leninskiy Prospekt, 59, 119333 Moscow, Russia; ontonic@gmail.com
- ⁴ Deutsches Elektronen-Synchrotron DESY, Notkestraße 85, 22607 Hamburg, Germany; dmitri.novikov@desy.de
- ⁵ Institute of Physics, Technische Universität Chemnitz, Reichenhainer Straße 70, 09126 Chemnitz, Germany; sibylle.gemming@physik.tu-chemnitz.de
- * Correspondence: matthias.zschornak@physik.tu-freiberg.de
- † These authors contributed equally to this work.



Citation: Ludt, C.; Ovchinnikova, E.; Kulikov, A.; Novikov, D.; Gemming, S.; Meyer, D.C.; Zschornak, M. Interactions of Ruddlesden-Popper Phases and Migration-Induced Field-Stabilized Polar Phase in Strontium Titanate. *Crystals* **2021**, *11*, 693. <https://doi.org/10.3390/cryst11060693>

Academic Editors: Christian Rodenbücher, Carsten Korte and Qingping Fang

Received: 18 May 2021
Accepted: 7 June 2021
Published: 17 June 2021

Publisher’s Note: MDPI stays neutral with regard to jurisdictional claims in published maps and institutional affiliations.



Copyright: © 2020 by the authors. Licensee MDPI, Basel, Switzerland. This article is an open access article distributed under the terms and conditions of the Creative Commons Attribution (CC BY) license (<https://creativecommons.org/licenses/by/4.0/>).

Abstract: This work focuses on the validation of a possible connection of the known Ruddlesden-Popper (RP) phases and the novel concept of the migration-induced field-stabilized polar (MFP) phase. To study this subject, model structures of RP phases in bulk strontium titanate are analyzed by means of density functional theory (DFT). The obtained geometries are compared to experimental MFP data. Good agreement can be found concerning atomic displacements in the pm range and lattice strain inferred by the RP phases. Looking at the energy point of view, the defect structures are on the convex hull of the Gibb’s free energy. Although the dynamics to form the discussed defect models are not addressed in detail, the interplay and stability of the described defect model will add to the possible structure scenarios within the near-surface region of strontium titanate. As a result, it can be suggested that RP phases generally favor the MFP formation.

Keywords: perovskites; transition metal oxides; defect structures; phase transition; MFP phase; RP phases; density functional theory

1. Introduction

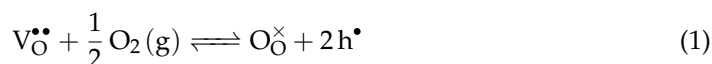
Strontium titanate as a representative of transition metal oxides has been in the focus of research for many years. The lattice parameter of $a = 3.905 \text{ \AA}$ matches with a variety of materials. High and anisotropically strain-dependent dielectric constant [1] and a large-scale tunability of electric, [2,3] dielectric, and optical properties [4,5] make strontium titanate an interesting substrate material for, e.g., the growth of ferroelectric thin films [6], ferroelectric tunnel junctions [7], high- T_c superconducting or colossal magnetoresistive films [8–10]. Recent work on strontium titanate promises a further application as resistance switching random access memory [11,12]. In the literature [12–14] there are several explanations for the switching mechanisms proposed, among others, conducting filaments [11,15], phase transitions [16–18], alteration of potential barriers [19], and charge carrier trapping [20,21]. Hanzig et al. [22–25] introduced a new approach, postulating a new phase, which forms during electroformation: the so-called migration-induced field-stabilized polar (MFP) phase. Richter et al. [26] analyzed the MFP phase with Resonantly Suppressed Diffraction (RSD), a new approach of Resonant X-ray Diffraction. With this method they were able to determine atomic displacements in strontium titanate on the

picometer scale during phase transformation. Furthermore, they found a dependency between strain and the displacements.

1.1. Defects in Strontium Titanate

The electronic structure and with it the physical properties of the crystals are strongly influenced by defects. In the case of strontium titanate there has been broad research to clarify how point defects like intrinsic oxygen vacancies [3,11,27,28], line defects such as screw dislocations [29,30] and two-dimensionally extended grain boundaries [31–36], as well as stacking faults [36–38] affect both [10].

The low energy of formation [39–43] and high coefficients for diffusion [44–47] as well as migration [24,48,49] make oxygen vacancies the predominately migrating species in strontium titanate. They are formed upon oxygen exchange with the atmosphere, if strontium titanate is stored at elevated temperatures. The reaction is described by Equation (1) in Kröger–Vink notation [50],



as the dynamic balance between the crystal with occupied oxygen sites ($\text{O}_{\text{O}}^{\times}$) and oxygen vacancies ($V_{\text{O}}^{\bullet\bullet}$) and the oxygen in the gas phase (h^{\bullet} denotes a defect electron/hole). Under reducing condition and temperatures above 750 °C, free charge carriers, i.e., electrons, are introduced due to charge compensation, causing *n*-type conductivity [22]. The picture of an ideal crystal interacting with the gas phase has to be seen as a model approach. The presence of oxygen getters as electrode materials may sensitively affect the local oxygen partial pressure in the surface region and even lead to decomposition [51]. $V_{\text{O}}^{\bullet\bullet}$ in strontium titanate changes the valence state of the titanium ion from 4+ to 3+ and the coordination from octahedral to pyramidal. The activation energy of oxygen vacancies in undoped strontium titanate is given in the literature [52] with E_{A} in the range of 0.62 eV–0.67 eV.

The reaction of the surface with the atmosphere described above is one possible mechanism introducing non-stoichiometry into the crystal. Beyond that, surface reactions and concomitant occurrence of extended defects within the near-surface region have attracted major interest in recent decades. Investigations based on transmission electron microscopy [53–55] as well as comparison to neutron diffraction data [56] give direct proof of their existence and high concentration in this region. Extensive work has also revealed their role in resistive switching mechanisms in strontium titanate crystals [11,57] and related oxide systems [13]. In addition, dislocations may act as fast diffusion paths for strontium transport [58], which is strongly inhibited for vacancy processes in the ideal structure [59]. In consequence, accumulations of SrO micro-crystals are evidenced on the respective exits at the surface, described by Szot et al. [57,60]. The redistribution of oxygen within the crystal in the presence of an electric field and concomitant changes in local composition may lead to local transient phases, e.g., the MFP phase [22], as well as stable phases, e.g., the homologous series of Ruddlesden-Popper (RP) phases [14,61], whose interactions are studied here.

1.2. Ruddlesden-Popper Phases

RP phases are crystallographic shear structures. Since Ruddlesden and Popper [38] introduced the first structure with respect to strontium titanate in 1958, there had been further research [10,62–64]. Early studies [62,65] predicted the stability of the first elements of this series and suggested that strontium titanate adapts to non-stoichiometry in its structure with the formation of RP phases, following the sum formula $\text{SrO}(\text{SrTiO}_3)_n$ in which additional SrO planes appear as ordered SrO-OSr stacking faults. The change in sum formula is accompanied by a change of the space group from $\text{Pm}\bar{3}\text{m}$ for bulk strontium titanate to $I4/m\bar{m}\bar{m}$. The structures can be found in the quasi-binary phase diagram SrO-TiO₂ which is given in Figure 1. An illustration of the compositional boundaries, strontium oxide and strontium titanate, as well as RP phases $n = 1$ –3 is given in Figure 2.

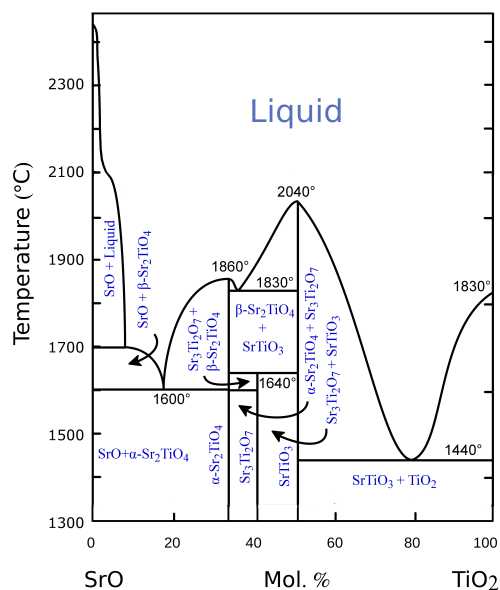


Figure 1. Quasi-binary phase diagram of SrO-TiO₂. Next to the compositional boundaries SrO (0 Mol.%) and SrTiO₃ (50 Mol.%) intermediate phases appear, the so-called Ruddlesden-Popper (RP) phases SrO(SrTiO₃)_n, e.g., Sr₂TiO₄ with n = 1 at 33.3 Mol.% and Sr₃Ti₂O₇ with n = 2 at 40 Mol.%. Redrawn from Ropp [66].

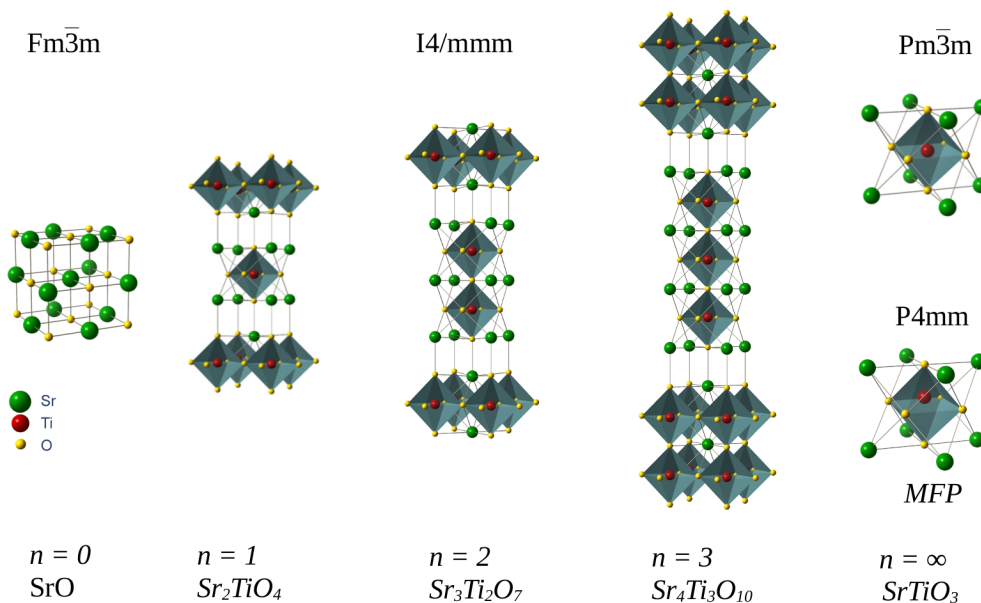


Figure 2. Unit cells of the homologous series of Ruddlesden-Popper (RP) phases SrO(SrTiO₃)_n n = 0–3, ∞ and the MFP phase (atomic displacements exaggerated). Redrawn from Zschornak et al. [10].

1.3. Migration-Induced Field-Stabilized Polar Phase

Based on the redistribution of oxygen vacancies in the strontium titanate lattice, Hanzig et al. [22] suggested a new phase, which is built during electroformation: The so-called MFP phase. The process of the phase transition is given in the following:

Considering a doubled unit cell of strontium titanate in thermodynamic equilibrium without an applied electric field ($E = 0$), the introduction of an oxygen vacancy alters the Ti-O octahedra of both unit cells into pyramids. Hanzig et al. [22] showed in terms of DFT calculations that the Ti ions are moving away from the neutral oxygen vacancy towards the top of the pyramids while oxygen ions move in the opposite direction. By applying an

electric field ($E > 0$), the Ti^{3+} ions of both pyramids move in the field direction while the O ions move against it, devising two different scenarios of atomic displacements with a break of the initial inversion symmetry at the position of the vacancy. The vacancy drifts towards the cathode via site exchange with oxygen ions on a lattice site, so one unit cell remains without point defects. Furthermore, it is proposed that in this unit cell the Ti ion maintains the displacement out of the center position and therefore a dipole moment is established, as long as the electric field is applied. Displacements in other directions are energetically unfavored and cannot establish. The new phase is polar and it is described as migration-induced field-stabilized polar phase, reflecting the process of its formation.

2. Motivation and Aims

The present work focuses on the investigation and validation of an interplay between possible Ruddlesden-Popper (RP) phases and the MFP phase. To study if the MFP phase may be induced by singular stacking faults of the RP phases, the three thermodynamically stable RP compounds ($n = 1-3$) are assumed to be embedded in bulk strontium titanate. Experimentally determined structure data obtained on the MFP phase by resonant X-ray diffraction [26], i.e., lattice parameters and atomic positions, should be reproduced theoretically by density functional theory (DFT) calculations with supercells of embedded RP phases. The validation of the strain which the RP phase induces onto the stoichiometric strontium titanate is in focus of the comparison of experimental and theoretical data. It is assumed that this perturbation may be sufficient to alter the crystal structure of the cubic SrTiO_3 to a ferroelectric phase.

We are aware that with this approach we can only assess the final defect state with simultaneous occurrence of MFP and RP phases as a scenario, but we cannot reflect the dynamics which lead to this state. In particular, the redistribution of ionic species and respective adjustment of non-stoichiometry will play a crucial role here. In conjunction, the presence of extended defects in the near-surface region, such as dislocations, may be essential as fast Sr diffusion paths. The SrO-rich dislocation cores can even be considered as nano-stacking faults which classify as precursors of $\text{SrO}(\text{SrTiO}_3)_n$ phases [53]. This picture of an accompanied transformation of SrO-rich dislocations into RP phases also supports the experimental observation of MFP phase forming in the near-surface region instead of the rather perfect bulk region of the crystal [22].

3. Method

Periodic supercells are built from the respective RP phase which is continuous in b -direction and surrounded with five layers of bulk strontium titanate in a -direction (see Figure 3). The number of strontium titanate layers in c -direction is aligned to the different c -parameters in the series of RP phases, i.e., 3, 5, and 7 cubic unit cells SrTiO_3 . To make the supercells chemically consistent, considering valence states and stacking orders in the interface areas in a -direction, minor changes were made in form of SrO buffer layers (inner blue box in Figure 3), so that the resulting structures obey the sum formula $\text{SrO}_m(\text{SrTiO}_3)_n$, i.e., $\text{Sr}_{24}\text{Ti}_{18}\text{O}_{60}$ (RP1), $\text{Sr}_{39}\text{Ti}_{31}\text{O}_{101}$ (RP2) and $\text{Sr}_{54}\text{Ti}_{44}\text{O}_{142}$ (RP3).

Additionally, a structure with further strontium titanate layers in a -direction is taken into account for the RP phase with $n = 1$ to see how the effect of the RP phase on the strontium titanate unit cells propagates for bigger structures in approximation of the diluted case. This structure with sum formula $\text{Sr}_{30}\text{Ti}_{24}\text{O}_{78}$ will be referred to as RP1^+ in the following.

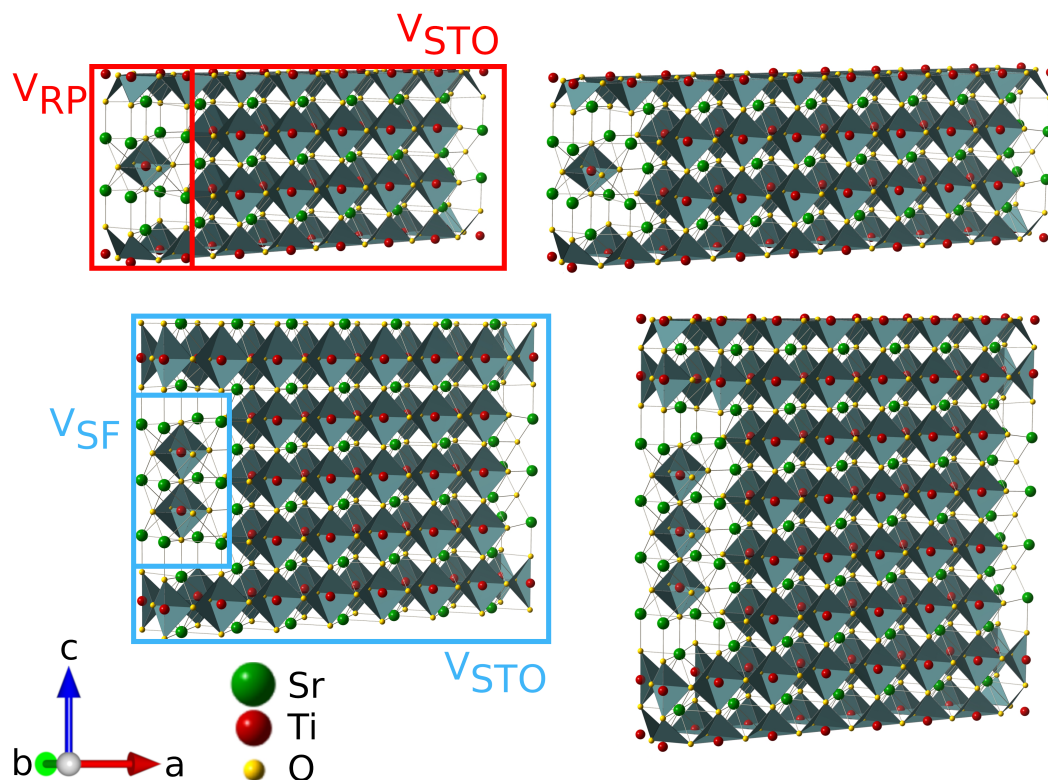


Figure 3. The initial supercell structures: the respective RP phases (left side) are embedded in bulk strontium titanate. The supercells are continuous in b -direction and surrounded by five layers of bulk strontium titanate in a -direction. The elongation in c -direction is given by the RP phase, i.e., 3, 5, and 7 cubic unit cells strontium titanate. Top left: $\text{Sr}_{24}\text{Ti}_{18}\text{O}_{60}$ (RP1), top right: $\text{Sr}_{30}\text{Ti}_{24}\text{O}_{78}$ (RP1⁺), bottom left: $\text{Sr}_{39}\text{Ti}_{31}\text{O}_{101}$ (RP2), bottom right: $\text{Sr}_{54}\text{Ti}_{44}\text{O}_{142}$ (RP3), Sr: green, Ti: red, O: yellow. The colored boxes mark the considered volume ratios $V_{\text{RP}}/V_{\text{STO}}$ in red and $V_{\text{SF}}/V_{\text{STO}}$ in blue.

All the electronic structure calculations were performed using DFT as it is implemented in the VASP code. Potentials were treated in the projector augmented wave (PAW) method and the exchange correlation energy is approximated in generalized gradient approximation (GGA) with the Perdew–Burke–Ernzerhof (PBE) parametrization. The total energy convergence criterion was set to 10^{-9} eV with a maximum kinetic energy for the plane wave basis set of 450 eV. The sampling in k -space was realized by Γ centered Monkhorst-Pack grids with $2 \times 12 \times 4$ for the RP1 supercell and $2 \times 12 \times 2$ for the RP2 and RP3 supercells, to achieve comparable k -point spacing. For the relaxation, in addition to the c -parameter, all degrees of freedom regarding the atomic positions are given while the lattice parameters in a - and b -direction are kept fixed to account for the clamping by the bulk. The convergence criterion for forces was set to 10^{-4} eV/Å.

4. Results

4.1. The Macroscopic Point of View

The c -Parameter

In Table 1 the relaxed lattice parameter c as well as its deviation $\Delta c = c_{\text{sc,rel}} - m \cdot c_{\text{STO,rel}}$ and the relative deviation $\Delta c/c$ are listed. Here, $c_{\text{sc,rel}}$ and $c_{\text{STO,rel}}$ are the relaxed lattice parameters of the supercell and of strontium titanate, respectively, and m is the number of strontium titanate units in the supercell, i.e., 3, 5, 7 for the systems RP1/RP1⁺, RP2 and RP3.

Table 1. Relaxed lattice parameter c , deviation Δc and relative deviation $\Delta c/c$. All structures are stretched in c -direction but the relative deviation $\Delta c/c$ gets smaller as n increases.

	c [Å]	Δc [Å]	$\Delta c/c$ [%]
RP1	12.23	0.69	5.66
RP1 ⁺	12.17	0.64	5.25
RP2	20.25	1.03	5.06
RP3	28.28	1.37	4.84

An increase of the initial lattice parameter c is evident for all supercells. Comparing the structures RP1 and RP1⁺, it shows that the increased number of strontium titanate layers compensates the stress better, which the RP phase embedded in the supercell induces onto the SrTiO₃ cubic unit cells, resulting in a smaller Δc value. The ratio $\Delta c/c$ exhibits a trend to smaller values along the series of RP phases embedded in the supercells.

In Figure 4 $\Delta c/c$ is plotted against the two different volume ratios. One is given by the volume of the RP phases V_{RP} compared to the volume of bulk strontium titanate V_{STO} , represented in Figure 3 with the red box. So the ratio is 2/5 for the supercells RP1, RP2, and RP3 and 2/7 for the supercell RP1⁺. On the other hand, the volume ratio is based on the relation of SrO to STO units in the supercells. The ratios here are 6/18, 6/24, 8/31, and 10/44 for the supercells RP1, RP1⁺, RP2, and RP3, respectively. The horizontal cyan line marks the experimental value given by Richter et al. [26] and represents $\Delta c/c$ values measured for the MFP phase by X-ray diffraction.

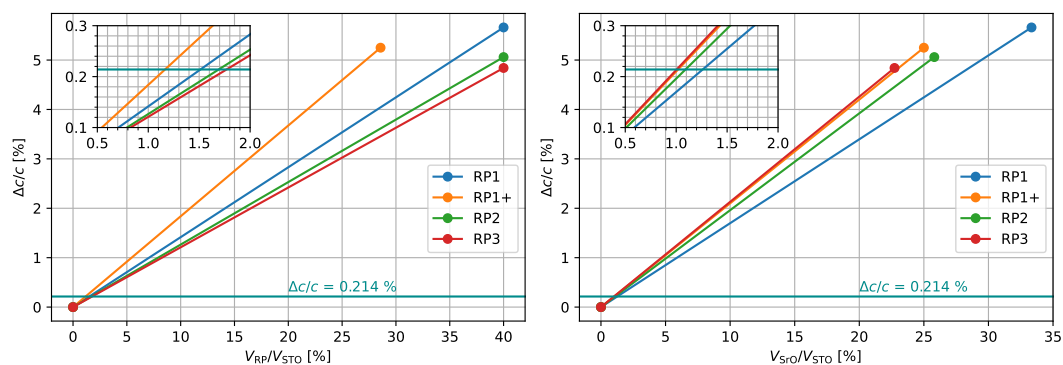


Figure 4. $\Delta c/c$ against the volume ratio V_{RP}/V_{STO} and the ratio V_{STO}/V_{STO} for the supercell models with implemented RP phases $n = 0-3$. The linear approximations are included as a guide to the eye to estimate the confidence region at the strain level of the experimental $\Delta c/c$ value [26] (horizontal cyan line).

The respective volume ratios V_x/V_{STO} determined from the intersections of the experimental data with the extrapolation of our $\Delta c/c$ values (see Figure 4) are given in Table 2. On the basis of the calculated data and the assumption that in first order approximation the dependencies are linear, they represent the volume ratio which is needed to compensate the stress induced by the RP phase to achieve the MFP phase conditions. Since the origin of their strain versus volume ratio dependency is fixed, the region of confidence becomes narrower for smaller defect concentration. It can clearly be seen that a high dilution and, respectively, a small defect concentration is necessary to meet the experimental MFP data.

Following these data, the respective ratios for both considered models account to about 1%. This result is close to the simple estimate of a ratio from the experimental c parameters of the individual phases, e.g., a ratio of 1.2% for $c_{RP1} = 12.571$ Å [67] and $c_{STO} = 3.905$ Å.

Table 2. V_x/V_{STO} according to Figure 4 to achieve experimental strains of the MFP phase for both ratio definitions.

	$V_{\text{RP}}/V_{\text{STO}}$ [%]	$V_{\text{SrO}}/V_{\text{STO}}$ [%]
RP1	1.5	1.3
RP1 ⁺	1.2	1.0
RP2	1.7	1.1
RP3	1.8	1.0

4.2. Distortions of TiO_6 Octahedra

In general, the electronic properties of transition metal oxides are most dependent on the dispersion of the transition metal d-states. In real space this corresponds to the TiO_6 octahedra and slight deviations from the local cubic perovskite structure in bond distances and angles. In the following these parameters are discussed in detail. The atomic displacements in c -direction are of particular interest, since they determine the potential electric polarization in the presence of an electric field perpendicular to the surface of the crystals. The deviation of the unit cell is also one important experimental observation, considering the mechanisms occurring during formation of MFP phase. In the literature [26] the increase of the Sr-Ti distance in the c -direction after MFP phase formation is given with a value of 1.34 pm, obtained by RSD. In Figure 5 the c -component of the distances for all nearest neighbors in the unit cells are plotted along the a -direction, taking the center of the RP phase in the structure as origin. The distances are calculated for all neighbors in a radius of 3.4 Å and an averaged Sr layer position. So the resulting average distances are comparable to the experimental RSD findings, which predict a shift out of the equilibrium position of 1.34 pm for Ti, 3.67 pm for O in the Sr plane and 3.8 pm for O in the Ti plane.

In Table 3 the mean values of the supercells are listed as well as the experimental values. Considering that our calculations represent displacements at a temperature of 0 K neglecting thermal expansion effects, a good general agreement between the experiment and the trend of our model can be found.

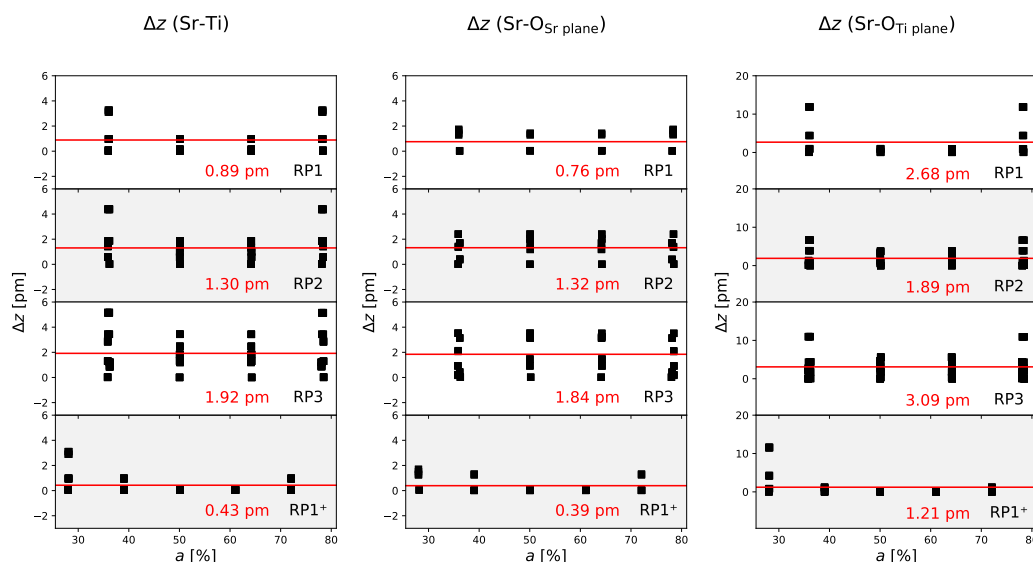
**Figure 5.** Δz of Sr-Ti, Sr-O distances in the supercells along a -direction. The red line represents the mean values. For RP1⁺ the supercell is longer in a , thus, on a relative scale the atomistic planes are denser.

Table 3. Differences of the z-component of the Sr-Ti distance and the Sr-O distances for both Wyckoff positions between bulk and strained strontium titanate cells, for the calculated supercells and the respective experimental average values.

	Sr-Ti [pm]	Sr-O _{Sr} [pm]	Sr-O _{Ti} [pm]
RP1	0.89	0.76	2.68
RP1 ⁺	0.43	0.39	1.21
RP2	1.30	1.32	1.89
RP3	1.92	1.84	3.09
exp. value [26]	1.34	3.67	3.80

4.3. The Microscopic Point of View

4.3.1. Sr-Sr-Distances

To evaluate the atomistic distortions within the microscopic SrTiO₃ cells, average values of the lattice parameters of the strained cells in the bulk region have been obtained from the modeled supercells. For this purpose all physically plausible distances between neighboring strontium ions in a radius between 3 Å and 4.5 Å have been analyzed. A minimum of 3 Å was introduced to eliminate double counting for the distance of 0 Å and filter out smaller distances which appear in the embedded RP phase, whereas the maximum of 4.5 Å was introduced to find only nearest neighbors. The results are listed in Table 4.

Table 4. Relative changes of the lattice parameters of the SrTiO₃ unit cells in the bulk area in percent, calculated from the Sr-Sr distances. The strain is induced by fixing two lattice parameters to SrTiO₃ bulk values and a relaxational degree of freedom in the third dimension, emulating the incorporation of embedded RP stacking faults in an MFP layer perpendicular to the interface with bulk SrTiO₃.

	$\Delta a_{\text{STO}}/a_{\text{STO}}$ [%]	$\Delta c_{\text{STO}}/c_{\text{STO}}$ [%]	$\Delta V_{\text{STO}}/V_{\text{STO}}$ [%]
RP1	−2.24	6.00	3.64
RP1 ⁺	−1.72	5.33	3.52
RP2	−2.37	4.53	2.05
RP3	−2.42	4.14	1.62

It is evident that the SrTiO₃ cubic unit cells in the bulk region (right region of the red box in Figure 3) become compressed in *a*-direction and stretched in *c*-direction, while symmetry restricts a change in *b*-direction; whereby the change is bigger in *c* than in *a*. Comparing $\Delta c_{\text{STO}}/c_{\text{STO}}$ obtained here with the $\Delta c/c$ values listed in Table 1, the same magnitude is found for all structures, with a slight increase due to the off-centering of the Sr positions. The deviations are smaller than the picometer scale and the same trend to smaller changes appears.

Looking at $\Delta a_{\text{STO}}/a_{\text{STO}}$ there is also a trend apparent as *n* increases: Here, the absolute values of $\Delta a_{\text{STO}}/a_{\text{STO}}$ increase slightly for higher ordered RP phases. For both $\Delta c_{\text{STO}}/c_{\text{STO}}$ and $\Delta a_{\text{STO}}/a_{\text{STO}}$ the comparison of RP1 and RP1⁺ shows that the changes become smaller, as expected. The stress induced by the RP phase is compensated by more cubic unit cells SrTiO₃ in this case. The relative changes in volume are given in Table 4 as well. Based on this data, an increase of volume of a few percent is evident, which decreases for larger *n* of the embedded RP phase in the supercells.

In Figure 6 $\Delta a_{\text{STO}}/a_{\text{STO}}$ is plotted against the volume ratio which is indicated in Figure 3 by the red box. The volume ratio of SrO cells to STO cells in *a*-direction yields the same results. The horizontal cyan line marks the minimal stress for the ferroelectric transition following Haeni et al. [68]. They predicted the dependency of the ferroelectric transition of strontium titanate on temperature and in-plane strain $\epsilon_s = (a_{\parallel} - a_0)/a_0$ with a minimum compressive strain for the ferroelectric phase at 0 K of $\Delta a/a = -0.55\%$. The calculated $\Delta a_{\text{STO}}/a_{\text{STO}}$ values of -1.7% to -2.4% imply ferroelectricity for the stressed SrTiO₃ unit cells in all supercells. Taking into account the estimated dilution of about two

orders of magnitude from the experimental data, the results indicate nonuniform transition regions to the polar phase around the stacking faults rather than homogeneous layers as might be expected from the constant strain in c -direction.

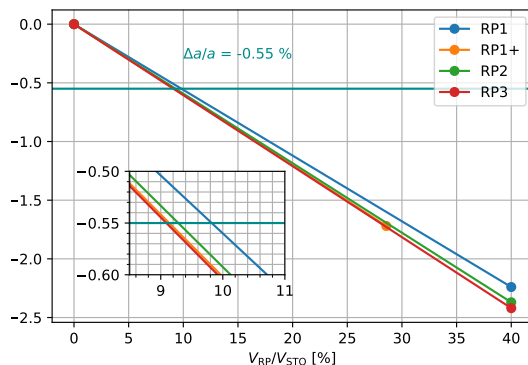


Figure 6. $\Delta a_{\text{STO}}/a_{\text{STO}}$ against the volume ratio $V_{\text{RP}}/V_{\text{STO}}$ for the RP phases with $n = 0-3$. The linear approximations are included as a guide to the eye to estimate the confidence region at the strain level of the experimental $\Delta a/a$ value [68] for an exclusively strain-induced ferroelectric transition in strontium titanate (horizontal cyan line).

In Table 5 the ratios $V_{\text{RP}}/V_{\text{STO}}$ of the intersections are listed. Following these data, an exclusively strain-induced ferroelectric transition would occur for supercells with $V_{\text{RP}}/V_{\text{STO}} > 9\%$. In this picture, bond distortions and respective atomic displacements due to the atomistic vicinity are not yet taken into account. These effects will be discussed in the following section.

Table 5. $V_{\text{RP}}/V_{\text{STO}}$ values according to Figure 6 to achieve ferroelectric strontium titanate following the approach by Haeni et al. [68].

	$V_{\text{RP}}/V_{\text{STO}}$ [%]
RP1	9.9
RP1 ⁺	9.1
RP2	9.2
RP3	9.1

4.3.2. Breaking the Symmetry

There is another important issue, which is still to be analyzed: The atomic distortions discussed above only show the absolute strain values of the individual SrTiO_3 cells. An important proposition of Hanzig et al. [22] is the break of centrosymmetry and with it a polarization of the unit cell during the formation of the MFP phase. To have a closer look at this behavior, Figure 7 shows the data presented in Figure 5 as histogram. Here the shift is distinguished by the sign: the positive Δz values are plotted in positive and the negative in negative y -direction, the red lines show the equilibrium values of bulk strontium titanate.

First of all it is evident that there is no continuous distribution of distances but a rather distinct agglomeration of certain values corresponding to specific locally distorted strontium titanate unit cells. In addition, there is an essential statement which can be derived from this diagrams: The distributions are nearly symmetrical for positive and negative distances. This means a rather small break of inversion symmetry in the strontium titanate unit cells occurs due to the strain implied by the embedded RP phases itself. To influence bulk strontium titanate by the introduced defects towards MFP phase properties the according atomic deviations are found to be present, but there is still the necessary condition of an electric field to be applied to obtain the polar characteristics. The respective energy barriers for the ionic ordering which have to be overcome by thermal activation to

form the polar MFP phase might explain the slow dynamics of the formation on the order of hours, as has been observed in [22].

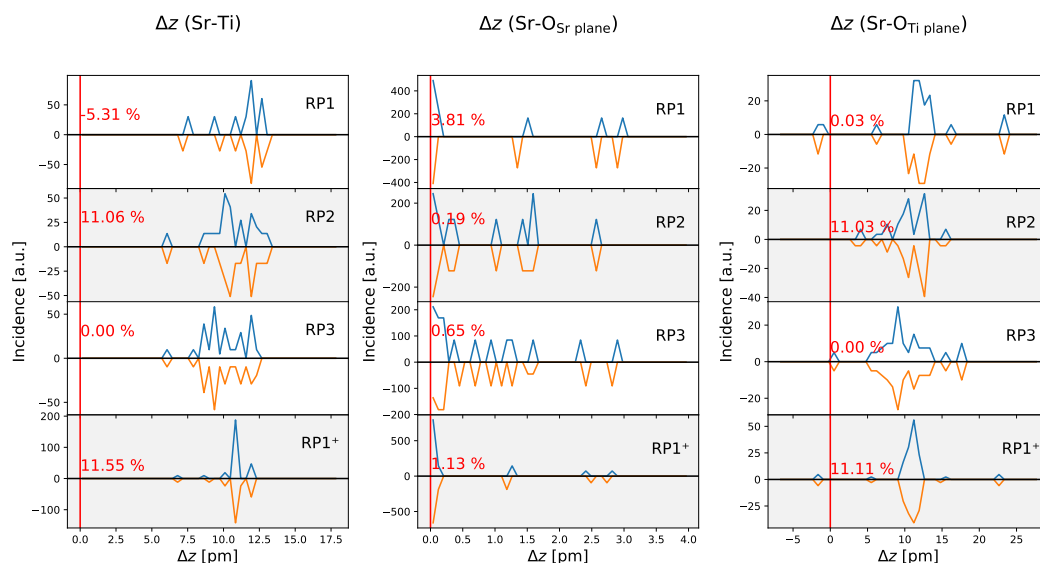


Figure 7. Histogram of the z-component of Sr-Ti distances and Sr-O distances for both wyckoff positions. The red line marks the equilibrium values of bulk strontium titanate. The relative differences between positive and negative values are also given by the red numbers.

4.4. The Energy Point of View

4.4.1. Energies of Formation and Defect Energies

In terms of stability adequate reference values are given by strontium oxide and strontium titanate, so atomic relaxations for these structures were performed in addition. In Table 6, the total energies of the oxides are presented next to the energies of the supercells. The energies of formation E_f are then calculated according to Equation (2).

$$E_f^{\text{RP}_{n,m}} = E[(\text{SrO})_m(\text{SrTiO}_3)_n] - n \cdot E[\text{SrTiO}_3] - m \cdot E[\text{SrO}] \quad (2)$$

The change in formation energy, compared to the binary oxide SrO and the ternary oxide SrTiO₃, is positive for all structures. The values vary between 1 eV and 2 eV, corresponding to about 50 meV per atom of the stacking fault. They may easily occur in pristine strontium titanate crystals with an electric field induced chemical gradient which is based on ionic redistribution, and associated with an oxygen partial pressure and respective compositional variation. It can be noted that the energy still decreases several percent by introducing more SrTiO₃ cubic unit cells, as it is done for the structure RP1 going to RP1⁺.

Furthermore, interface defect energies e_D have been calculated. For this the energy of formation is divided by the interfacial area. In the first defect picture, referring to the RP defect model as marked in red in Figure 3, this area corresponds to the product of the fixed b -parameter and the relaxed c -parameters (Table 1) multiplied by two to account for the twofold appearance of the interface region along a -direction incorporated for periodic boundary conditions. All values are positive and in magnitude of approximately 10 meV/Å². A trend towards smaller energies is apparent for higher orders of the embedded RP phases in the supercells. This can be expected, since there are always congruently intergrown layers of strontium titanate through the RP stacking faults. They get more numerous and higher in weight when going to higher orders n in the homologous series of RP phases.

Table 6. Total energies E_{tot} and energies of formation E_f following Equation (2). The additional columns give the values normalized to the numbers of atoms appearing in the stacking fault region E_f per atom SF, corresponding interface defect energies per area $e_{\text{D(RP)}}$ and $e_{\text{D(SF)}}$ with respect to both defect models, presented in Figure 3, as well as defect interface energies $E_{\text{D(RP)}}$ and $E_{\text{D(SF)}}$ normalized to the standard cubic phase of SrTiO₃.

	E_{tot} [eV]	E_f [eV]	E_f Per Atom SF [meV]	$e_{\text{D(RP)}}$ [meV/Å ²]	$E_{\text{D(RP)}}$ [meV]	$e_{\text{D(SF)}}$ [meV/Å ²]	$E_{\text{D(SF)}}$ [meV]
SrO	−16.780	-	-	-	-	-	-
SrTiO ₃	−43.001	-	-	-	-	-	-
RP1	−873.085	1.613	67.2	17.2	254	8.58	127
RP1 ⁺	−1131.183	1.533	63.9	16.4	242	8.19	121
RP2	−1465.763	1.523	47.6	9.78	145	4.89	72.3
RP3	−2058.131	1.733	43.3	7.97	118	3.98	58.9

In the second defect picture, the interface defect energies $e_{\text{D(SF)}}$ correspond to the stacking fault area as marked in blue in Figure 3, showing similar trends and order of magnitude. Based on these values, normalized defect interface energies have been calculated with respect to the bulk unit cell area of SrTiO₃ for both defect pictures, for better comparison. It is evident that those defect energies $E_{\text{D(RP)}}$ and $E_{\text{D(SF)}}$ are significantly smaller than the activation energy of oxygen vacancy migration ($E_A = 0.62$ eV– 0.67 eV [52]) or strontium vacancy migration ($E_A = 3.7$ eV / 2.9 eV via an oxygen vacancy [59]). This indicates that if compositional gradients exist in strontium titanate, e.g., due to migration of oxygen and strontium vacancies, RP phases may be embedded in bulk strontium titanate at the same time, without a large additional energy contribution for the formation. This also strengthens the scenario of a simultaneous appearance of MFP phase and RP phase in strontium titanate.

4.4.2. Density of States

Figure 8 presents the density of states (DOS) exemplarily for the supercell with RP1 and the corresponding RP phase. Within the DOS several areas can be separated. In the first area ranging from -20 eV to -13 eV, two main peaks can be distinguished. The first one located at lower energies is dominated by O 2s character and the other located at higher energies is dominated by Sr 4p orbitals. In the second area with a range of -5 eV to the Fermi energy O 2p orbitals prevail. The third area from 2 eV to 8 eV is dominated by Ti 3d orbitals. The band gaps of the oxides SrO and strontium titanate are given by 3.4 eV and 1.9 eV, respectively, with the usual underestimation of DFT [69]. As the strontium titanate character increases in the series SrO(SrTiO₃)_{*n*}, a trend appears in the series to smaller band gaps, as expected [10,70]. The band gaps are given with 2.01 eV, 1.99 eV, and 1.98 eV for RP1, RP2, and RP3, respectively. The band gaps of the supercells are all given by 1.9 eV. It is straightforward that they yield the band gap of strontium titanate considering the high volume ratio of strontium titanate in the supercells.

For further comparison, difference DOS have been calculated by subtracting the DOS of strontium oxide and strontium titanate with stoichiometric amounts from the DOS of the supercells. Again, exemplarily the difference DOS for the RP1 supercell is shown in Figure 8. The positive peaks correspond to the supercell's additional density, whereas the negative peaks correspond to the reduced character of strontium oxide and strontium titanate. For all difference DOS you find the same curve shape, as can be seen exemplarily for RP1, the formation of RP phases in bulk strontium titanate results in a stabilization of the O 2s states in the region of -18 eV to -16 eV, as these peaks shift to lower energies. For the peak corresponding to Sr 4p states in energy range of -16 eV to -13 eV the states broaden and show greater dispersion in the supercells. The third peak in the area of -5 eV up to the Fermi energy corresponds to O 2p and occupied Ti 3d states and exhibits broadening as well. Looking at it in detail, three subareas are distinguishable and each is

shifting to lower energies. The last peak in the region of 2 eV to 8 eV shows unoccupied Ti 3d states. These states also broaden in the supercells. A summary of the peak position and the character of the corresponding states is given in Table 7. In addition, the ratio of peak areas between the difference DOS and the DOS of the supercells is given.

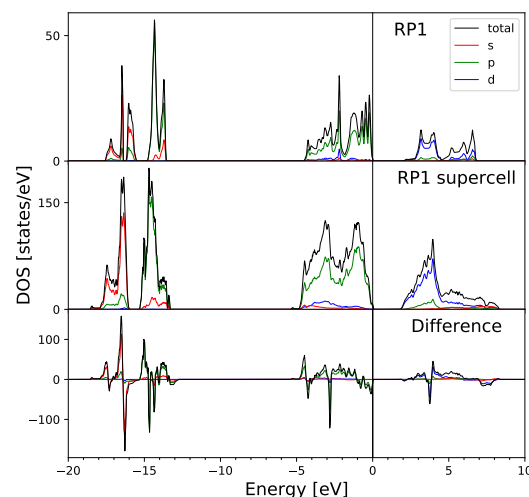


Figure 8. Density of states of the isolated RP phases, the supercell, and the difference DOS exemplarily for RP phase $n = 1$.

Multiplying the differences with the volume ratio of about 1%, as estimated above to reflect the experimental strain scenario for the MFP phase, it can be assessed whether these changes are measurable by high-resolution spectroscopic methods like X-ray Photoelectron Spectroscopy (XPS), Resonant X-ray Diffraction (RXD) [71], or X-ray Absorption Near Edge Structure (XANES) [72]. The results are in magnitude of 1000 ppm, so sensitive spectroscopic methods should be able to verify the differences calculated here.

Table 7. Peak position and character for the peaks in the DOS. The ratio $A_{\text{diff}} / A_{\text{tot}}$ is given by the corresponding peak areas of the difference DOS divided by the peak areas of the supercells.

#	Range [eV]	Character	RP1	$A_{\text{diff}} / A_{\text{tot}}$ [%]		
				RP1 ⁺	RP2	RP3
1	−18 to −16	O 2s	36	36	42	43
2	−16 to −13	Sr 4p	16	21	12	14
3	−5 to 0	O 2p, Ti 3d	14	14	15	15
4	2 to 8	Ti 3d	21	22	21	22

5. Conclusions and Outlook

In this work the concept of the MFP phase distribution in strontium titanate is analyzed with a new approach: The presence of RP phases in bulk strontium titanate could influence the conditions in such a system in the way that the formation of the MFP phase may be favored. With this scope, supercells of RP phases $\text{SrO}(\text{SrTiO}_3)_n$, with $n = 1-3$ embedded in bulk strontium titanate have been analyzed by use of DFT, to compare the results to experimental data recently obtained by RXD. By these means four structures were analyzed with the chosen DFT method. Although this approach cannot explain the dynamics of the MFP phase formation itself, especially the microscopic correlation to the ionic migration and respective boundary conditions for fast Sr transport such as extended defects in general, it compares the experimental evidence of the final atomistic bulk MFP structure and adds

the interaction with RP phases to the possible stable defect scenarios. Here the important results are summarized:

As expected, the energies of formation, tabulated in Table 6, suggest that the given systems are not energetically favored over the simultaneous presence of strontium oxide and strontium titanate. As the defect formation energies are an order of magnitude below the activation energy of oxygen vacancies and strontium vacancies, it can be concluded that if compositional changes occur by means of defect migration in an electric field, the given systems could form simultaneously to the MFP phase, with little energetic effort.

The strain is quantified which the embedded RP phase induces onto the strontium titanate unit cells in the bulk area of the supercell. Based on Table 4, it is apparent that the stressed SrTiO₃ cells are compressed in *a*-direction and stretched in *c*-direction. The effect is strongest for RP1 and lowers in the ascending series of the embedded RP phase supercells, which is shown based on the relative change of volume. Both strains promote the transition to the polar phase. Based on the relative change of the lattice parameter *c* the ratio of RP phase to volume could be estimated, which is needed to compensate the induced stress on the system by the embedded RP phase and to match the experimental findings presented in literature [26]. Here it is evident that the RP phase occupies only a small fraction of the total volume.

With the calculated displacements in the unit cell of SrTiO₃ in the systems a reasonable agreement with the experimental data from literature is found. The displacement of the distances of Sr-Ti as well as Sr-O show the desired trend. On the other hand, only a slight spontaneous break of centrosymmetry and associated electric polarization occurs in the strontium titanate unit cells of the supercells without application of an electric field. The histogram of the Sr-Ti distances shows a overall symmetric distribution of positive and negative values. It should be further noted that there are discrete agglomerations of atomic displacement values for all modeled structures, which strongly supports the idea of a potentially polar character.

Based on the difference DOS and the volume ratio of defect region to bulk strontium titanate, it can be expected that the shifts in the DOS, which occur when RP phases form in bulk strontium titanate, should be measurable by means of high-resolution spectroscopy in systems which reproduce MFP properties, by methods with a detection limit of about 1000 ppm.

Summarizing, the present study confirms the initial hypothesis that RP phases could simultaneously form in bulk strontium titanate during the formation of the MFP phase and may even promote this phase transition. There are also aspects with respect to this topic which deserve a separate in-depth treatment in further work: The effects of the embedded RP phase on the bulk SrTiO₃ unit cells could be analyzed for bigger supercells to ensure convergence. Concerning the DOS investigation, experimental data, possibly even resolved on a partial DOS level, would further strengthen the picture of RP stacking fault formation. As the symmetry break is not found by just stressing the cubic strontium titanate unit cells, it is straightforward that further DFT calculations with an artificial electric field are important to underline the results found here. Such calculations may prove the hypothesis that RP phases directly incorporate the polar properties of the MFP phase in SrTiO₃ crystals accompanied by the formation of a spontaneous electric polarization under the influence of an electric field, which would explain the polar properties of the MFP phase.

Author Contributions: Conceptualization, M.Z.; computations, formal analysis, and visualization, C.L.; methodology and validation, M.Z. and S.G.; resources, M.Z. and D.C.M.; writing—original draft preparation, C.L. and M.Z.; writing—review and editing, C.L., E.O., A.K., D.N., S.G., D.C.M., and M.Z.; supervision, project administration, and funding acquisition, M.Z.; All authors have read and agreed to the published version of the manuscript.

Acknowledgments: C.L., M.Z., and S.G. acknowledge funding by the DFG within the projects DFG 409743569, ZS 120/1-1 and DFG 405595647, GE 1202/12-1 and by the Helmholtz-Initiative and Networking funds (Ex Net-0028, W2/W3-026). E.O. and A.K. acknowledge further funding by the Russian Foundation for Basic Research (project No. 19-52-12029a).

Conflicts of Interest: The authors declare no conflict of interest.

References

1. Antons, A.; Neaton, J.B.; Rabe, K.M.; Vanderbilt, D. Tunability of the dielectric response of epitaxially strained SrTiO₃ from first principles. *Phys. Rev. B* **2005**, *71*, 116. [\[CrossRef\]](#)
2. Hui, S.; Petric, A. Electrical Properties of Yttrium-Doped Strontium Titanate under Reducing Conditions. *J. Electrochem. Soc.* **2002**, *149*, J1. [\[CrossRef\]](#)
3. Waser, R. Bulk Conductivity and Defect Chemistry of Acceptor-Doped Strontium Titanate in the Quenched State. *J. Am. Ceram. Soc.* **1991**, *74*, 1934–1940. [\[CrossRef\]](#)
4. Kulagin, N.A.; Dojcilovic, J.; Popovic, D. Valence State Stability in SrTiO₃ Doped with ME/RE-Ions. In *Physics of Laser Crystals*; Krupa, J.C., Kulagin, N.A., Eds.; Number volume 126 in NATO Science Series. Series II, Mathematics, Physics, and Chemistry; Kluwer Academic Publishers in cooperation with NATO Scientific Affairs Division: Bruxelles, Belgium, 2003; Volume 126, pp. 187–199. [\[CrossRef\]](#)
5. Hao, J.H.; Luo, Z.; Gao, J. Effects of substrate on the dielectric and tunable properties of epitaxial SrTiO₃ thin films. *J. Appl. Phys.* **2006**, *100*, 114107. [\[CrossRef\]](#)
6. Fong, D.D.; Stephenson, G.B.; Streiffer, S.K.; Eastman, J.A.; Auciello, O.; Fuoss, P.H.; Thompson, C. Ferroelectricity in ultrathin perovskite films. *Science* **2004**, *304*, 1650–1653. [\[CrossRef\]](#)
7. Kohlstedt, H.; Pertsev, N.A.; Rodríguez Contreras, J.; Waser, R. Theoretical current-voltage characteristics of ferroelectric tunnel junctions. *Phys. Rev. B* **2005**, *72*, 1623. [\[CrossRef\]](#)
8. Kwo, J.; Hsieh, T.C.; Fleming, R.M.; Hong, M.; Liou, S.H.; Davidson, B.A.; Feldman, L.C. Structural and superconducting properties of orientation-ordered Y₁Ba₂Cu₃O_{7-x} films prepared by molecular-beam epitaxy. *Phys. Rev. B* **1987**, *36*, 4039–4042. [\[CrossRef\]](#)
9. Mitsugi, F.; Ikegami, T.; Ebihara, K.; Narayan, J.; Grishin, A.M. Colossal magnetoresistive and ferroelectric thin films deposited by excimer laser induced plasma. *Sci. Technol. Adv. Mater.* **2001**, *2*, 525–531. [\[CrossRef\]](#)
10. Zschornak, M.; Gemming, S.; Gutmann, E.; Weißbach, T.; Stöcker, H.; Leisegang, T.; Riedl, T.; Tränkner, M.; Gemming, T.; Meyer, D.C. Surface modeling and chemical solution deposition of SrO(SrTiO₃)_n Ruddlesden–Popper phases. *Acta Mater.* **2010**, *58*, 4650–4659. [\[CrossRef\]](#)
11. Szot, K.; Speier, W.; Bihlmayer, G.; Waser, R. Switching the electrical resistance of individual dislocations in single-crystalline SrTiO₃. *Nat. Mater.* **2006**, *5*, 312–320. [\[CrossRef\]](#)
12. Sawa, A. Resistive switching in transition metal oxides. *Mater. Today* **2008**, *11*, 28–36. [\[CrossRef\]](#)
13. Waser, R.; Dittmann, R.; Staikov, G.; Szot, K. Redox-Based Resistive Switching Memories - Nanoionic Mechanisms, Prospects, and Challenges. *Adv. Mater.* **2009**, *21*, 2632–2663. [\[CrossRef\]](#)
14. Zschornak, M.; Hanzig, J.; Stöcker, H.; Leisegang, T.; Gemming, S.; Meyer, D. Structural transformation of the SrTiO₃ surface region due to electric fields at ambient temperature. In *Switching Effects in Transition Metal Oxides*; Roleder, K., Speier, W., Szot, K., Eds.; Wydawnictwo Naukowe PWN: Warszawa, Poland, 2021.
15. Janousch, M.; Meijer, G.L.; Staub, U.; Delley, B.; Karg, S.F.; Andreasson, B.P. Role of Oxygen Vacancies in Cr-Doped SrTiO₃ for Resistance-Change Memory. *Adv. Mater.* **2007**, *19*, 2232–2235. [\[CrossRef\]](#)
16. Beck, A.; Bednorz, J.G.; Gerber, C.; Rossel, C.; Widmer, D. Reproducible switching effect in thin oxide films for memory applications. *Appl. Phys. Lett.* **2000**, *77*, 139–141. [\[CrossRef\]](#)
17. Hamaguchi, M.; Aoyama, K.; Asanuma, S.; Uesu, Y.; Katsufuji, T. Electric-field-induced resistance switching universally observed in transition-metal-oxide thin films. *Appl. Phys. Lett.* **2006**, *88*, 142508. [\[CrossRef\]](#)
18. Liu, S.Q.; Wu, N.J.; Ignatiev, A. Electric-pulse-induced reversible resistance change effect in magnetoresistive films. *Appl. Phys. Lett.* **2000**, *76*, 2749–2751. [\[CrossRef\]](#)
19. Baikalov, A.; Wang, Y.Q.; Shen, B.; Lorenz, B.; Tsui, S.; Sun, Y.Y.; Xue, Y.Y.; Chu, C.W. Field-driven hysteretic and reversible resistive switch at the Ag–Pr_{0.7}Ca_{0.3}MnO₃ interface. *Appl. Phys. Lett.* **2003**, *83*, 957–959. [\[CrossRef\]](#)
20. Watanabe, Y.; Bednorz, J.G.; Bietsch, A.; Gerber, C.; Widmer, D.; Beck, A.; Wind, S.J. Current-driven insulator–conductor transition and nonvolatile memory in chromium-doped SrTiO₃ single crystals. *Appl. Phys. Lett.* **2001**, *78*, 3738–3740. [\[CrossRef\]](#)
21. Alvarado, S.F.; La Mattina, F.; Bednorz, J.G. Electroluminescence in SrTiO₃:Cr single-crystal nonvolatile memory cells. *Appl. Phys. A* **2007**, *89*, 85–89. [\[CrossRef\]](#)

22. Hanzig, J.; Zschornak, M.; Hanzig, F.; Mehner, E.; Stöcker, H.; Abendroth, B.; Röder, C.; Talkenberger, A.; Schreiber, G.; Rafaja, D.; et al. Migration-induced field-stabilized polar phase in strontium titanate single crystals at room temperature. *Phys. Rev. B* **2013**, *88*, 43. [[CrossRef](#)]
23. Hanzig, J.; Zschornak, M.; Nentwich, M.; Hanzig, F.; Gemming, S.; Leisegang, T.; Meyer, D.C. Strontium titanate: An all-in-one rechargeable energy storage material. *J. Power Sources* **2014**, *267*, 700–705. [[CrossRef](#)]
24. Hanzig, J.; Mehner, E.; Jachalke, S.; Hanzig, F.; Zschornak, M.; Richter, C.; Leisegang, T.; Stöcker, H.; Meyer, D.C. Dielectric to pyroelectric phase transition induced by defect migration. *New J. Phys.* **2015**, *17*, 023036. [[CrossRef](#)]
25. Khanbabaee, B.; Mehner, E.; Richter, C.; Hanzig, J.; Zschornak, M.; Pietsch, U.; Stöcker, H.; Leisegang, T.; Meyer, D.C.; Gorfman, S. Large piezoelectricity in electric-field modified single crystals of SrTiO₃. *Appl. Phys. Lett.* **2016**, *109*, 222901. [[CrossRef](#)]
26. Richter, C.; Zschornak, M.; Novikov, D.; Mehner, E.; Nentwich, M.; Hanzig, J.; Gorfman, S.; Meyer, D.C. Picometer polar atomic displacements in strontium titanate determined by resonant X-ray diffraction. *Nat. Commun.* **2018**, *9*, 178. [[CrossRef](#)] [[PubMed](#)]
27. Leisegang, T.; Stöcker, H.; Levin, A.A.; Weissbach, T.; Zschornak, M.; Gutmann, E.; Rickers, K.; Gemming, S.; Meyer, D.C. Switching Ti valence in SrTiO₃ by a dc electric field. *Phys. Rev. Lett.* **2009**, *102*, 087601. [[CrossRef](#)] [[PubMed](#)]
28. Stöcker, H.; Zschornak, M.; Leisegang, T.; Shakhverdova, I.; Gemming, S.; Meyer, D.C. Electric field mediated switching of mechanical properties of strontium titanate at room temperature. *Cryst. Res. Technol.* **2010**, *45*, 13–17. [[CrossRef](#)]
29. Jia, C.L.; Houben, L.; Urban, K. Atom vacancies at a screw dislocation core in SrTiO₃. *Philos. Mag. Lett.* **2006**, *86*, 683–690. [[CrossRef](#)]
30. Brunner, D. Low-temperature plasticity and flow-stress behaviour of strontium titanate single crystals. *Acta Mater.* **2006**, *54*, 4999–5011. [[CrossRef](#)]
31. Hutt, S.; Köstlmeier, S.; Elsässer, C. Density functional study of the Σ3 (111) [1̄10] symmetrical tilt grain boundary in SrTiO₃. *J. Phys. Condens. Matter* **2001**, *13*, 3949–3960. [[CrossRef](#)]
32. Astala, R.; Bristowe, P.D. A computational study of twist boundary structures in strontium titanate. *J. Phys. Condens. Matter* **2002**, *14*, 13635–13641. [[CrossRef](#)]
33. Zhang, Z.; Sigle, W.; Phillipp, F.; Rühle, M. Direct atom-resolved imaging of oxides and their grain boundaries. *Science* **2003**, *302*, 846–849. [[CrossRef](#)]
34. Zhang, Z.; Sigle, W.; de Souza, R.A.; Kurtz, W.; Maier, J.; Rühle, M. Comparative studies of microstructure and impedance of small-angle symmetrical and asymmetrical grain boundaries in SrTiO₃. *Acta Mater.* **2005**, *53*, 5007–5015. [[CrossRef](#)]
35. Lee, S.B.; Lee, J.H.; Cho, Y.H.; Kim, D.Y.; Sigle, W.; Phillipp, F.; van Aken, P.A. Grain-boundary plane orientation dependence of electrical barriers at Σ5 boundaries in SrTiO₃. *Acta Mater.* **2008**, *56*, 4993–4997. [[CrossRef](#)]
36. Benedek, N.A.; Chua, A.L.S.; Elsässer, C.; Sutton, A.P.; Finnis, M.W. Interatomic potentials for strontium titanate. *Phys. Rev. B* **2008**, *78*, 1639. [[CrossRef](#)]
37. Andersson, S.; Collén, B.; Kuylenstierna, U.; Magnéli, A.; Pestmalis, H.; Åsbrink, S. Phase Analysis Studies on the Titanium-Oxygen System. *Acta Chem. Scand.* **1957**, *11*, 1641–1652. [[CrossRef](#)]
38. Ruddlesden, S.N.; Popper, P. The compound Sr₃Ti₂O₇ and its structure. *Acta Crystallogr.* **1958**, *11*, 54–55. [[CrossRef](#)]
39. Moos, R.; Hardtl, K.H. Defect Chemistry of Donor-Doped and Undoped Strontium Titanate Ceramics between 1000° and 1400 °C. *J. Am. Ceram. Soc.* **1997**, *80*, 2549–2562. [[CrossRef](#)]
40. Uedono, A.; Shimayama, K.; Kiyohara, M.; Chen, Z.Q.; Yamabe, K. Study of oxygen vacancies in SrTiO₃ by positron annihilation. *J. Appl. Phys.* **2002**, *92*, 2697–2702. [[CrossRef](#)]
41. Neagu, D.; Irvine, J.T.S. Enhancing Electronic Conductivity in Strontium Titanates through Correlated A and B-Site Doping. *Chem. Mater.* **2011**, *23*, 1607–1617. [[CrossRef](#)]
42. Marrocchelli, D.; Sun, L.; Yildiz, B. Dislocations in SrTiO₃. *J. Am. Chem. Soc.* **2015**, *137*, 4735–4748. [[CrossRef](#)] [[PubMed](#)]
43. Stöber, M.; Cherkouk, C.; Leisegang, T.; Schelter, M.; Zosel, J.; Walter, J.; Hanzig, J.; Zschornak, M.; Prucnal, S.; Böttger, R.; Meyer, D.C. Oxygen Exchange Kinetics of SrTiO₃ Single Crystals. *Cryst. Res. Technol.* **2018**, *53*, 1800004. [[CrossRef](#)]
44. Paladino, A.E. Oxidation Kinetics of Single-Crystal SrTiO₃. *J. Am. Ceram. Soc.* **1965**, *48*, 476–478. [[CrossRef](#)]
45. Pasierb, P.; Komornicki, S.; Rekas, M. Comparison of the chemical diffusion of undoped and Nb-doped SrTiO₃. *J. Phys. Chem. Solids* **1999**, *60*, 1835–1844. [[CrossRef](#)]
46. Meyer, R.; Waser, R. Advances in point defect chemistry. *J. Eur. Ceram. Soc.* **2001**, *21*, 1743–1747. [[CrossRef](#)]
47. Zhang, L.; Liu, B.; Zhuang, H.; Kent, P.; Cooper, V.R.; Ganesh, P.; Xu, H. Oxygen vacancy diffusion in bulk SrTiO₃ from density functional theory calculations. *Comput. Mater. Sci.* **2016**, *118*, 309–315. [[CrossRef](#)]
48. Akhtar, M.J.; Akhtar, Z.U.N.; Jackson, R.A.; Catlow, C.R.A. Computer Simulation Studies of Strontium Titanate. *J. Am. Ceram. Soc.* **1995**, *78*, 421–428. [[CrossRef](#)]
49. Hanzig, J.; Zschornak, M.; Mehner, E.; Hanzig, F.; Münchgesang, W.; Leisegang, T.; Stöcker, H.; Meyer, D.C. The anisotropy of oxygen vacancy migration in SrTiO₃. *J. Physics. Condens. Matter Inst. Phys. J.* **2016**, *28*, 225001. [[CrossRef](#)] [[PubMed](#)]
50. Kröger, F.; Vink, H. Relations between the concentrations of imperfections in crystalline solids. *Solid State Phys.* **1956**, *3*, 307–435. [[CrossRef](#)]
51. Rodenbücher, C.; Meuffels, P.; Speier, W.; Ermrich, M.; Wrana, D.; Krok, F.; Szot, K. Stability and Decomposition of Perovskite-Type Titanates upon High-Temperature Reduction. *Phys. Status Solidi (Rrl) Rapid Res. Lett.* **2017**, *11*, 1700222. [[CrossRef](#)]
52. De Souza, R.A. Oxygen Diffusion in SrTiO₃ and Related Perovskite Oxides. *Adv. Funct. Mater.* **2015**, *25*, 6326–6342. [[CrossRef](#)]

53. Jia, C.L.; Thust, A.; Urban, K. Atomic-Scale Analysis of the Oxygen Configuration at a SrTiO₃ Dislocation Core. *Phys. Rev. Lett.* **2005**, *95*, 225506. [[CrossRef](#)]
54. Jin, L.; Guo, X.; Jia, C. TEM study of <110> -type 35.26° dislocations specially induced by polishing of SrTiO₃ single crystals. *Ultramicroscopy* **2013**, *134*, 77–85. [[CrossRef](#)]
55. Szot, K.; Rodenbücher, C.; Bihlmayer, G.; Speier, W.; Ishikawa, R.; Shibata, N.; Ikuhara, Y. Influence of Dislocations in Transition Metal Oxides on Selected Physical and Chemical Properties. *Crystals* **2018**, *8*, 241. [[CrossRef](#)]
56. Wang, R.; Zhu, Y.; Shapiro, S.M. Structural Defects and the Origin of the Second Length Scale in SrTiO₃. *Phys. Rev. Lett.* **1998**, *80*, 2370–2373. [[CrossRef](#)]
57. Szot, K.; Bihlmayer, G.; Speier, W. Chapter Four-Nature of the Resistive Switching Phenomena in TiO₂ and SrTiO₃: Origin of the Reversible Insulator–Metal Transition. *Solid State Phys.* **2014**, *65*, 353–559. [[CrossRef](#)]
58. Rhodes, W.H.; Kingery, W.D. Dislocation Dependence of Cationic Diffusion in SrTiO₃. *J. Am. Ceram. Soc.* **1966**, *49*, 521–526. [[CrossRef](#)]
59. Walsh, A.; Catlow, C.R.A.; Smith, A.G.H.; Sokol, A.A.; Woodley, S.M. Strontium migration assisted by oxygen vacancies in SrTiO₃ from classical and quantum mechanical simulations. *Phys. Rev. B* **2011**, *83*, 220301. [[CrossRef](#)]
60. Szot, K.; Speier, W.; Breuer, U.; Meyer, R.; Szade, J.; Waser, R. Formation of micro-crystals on the (100) surface of SrTiO₃ at elevated temperatures. *Surf. Sci.* **2000**, *460*, 112–128. [[CrossRef](#)]
61. Bobeth, M.; Farag, N.; Levin, A.A.; Meyer, D.C.; Pompe, W.; Romanov, A.E. Reversible Electric Field-Induced Structure Changes in the Near-Surface Region of Strontium Titanate. *J. Ceram. Soc. Jpn.* **2006**, *114*, 1029–1037. [[CrossRef](#)]
62. Udayakumar, K.R.; Cormack, A.N. Structural Aspects of Phase Equilibria in the Strontium-Titanium-Oxygen System. *J. Am. Ceram. Soc.* **1988**, *71*, C469–C471. [[CrossRef](#)]
63. Zschornak, M. Defect-Induced Local Electronic Structure Modifications within the System SrO–SrTiO₃–TiO₂. Ph.D. Thesis, TU Bergakademie Freiberg, Freiberg, Germany, 2015.
64. Jacob, K.; Rajitha, G. Thermodynamic properties of strontium titanates: Sr₂TiO₄, Sr₃Ti₂O₇, Sr₄Ti₃O₁₀, and SrTiO₃. *J. Chem. Thermodyn.* **2011**, *43*, 51–57. [[CrossRef](#)]
65. Udayakumar, K.R.; Cormack, A.N. Non-stoichiometry in alkaline earth excess alkaline earth titanates. *J. Phys. Chem. Solids* **1989**, *50*, 55–60. [[CrossRef](#)]
66. Ropp, R.C. *Encyclopedia of the Alkaline Earth Compounds*; Elsevier: Hoboken, NJ, USA, 2013.
67. Gutmann, E.; Levin, A.A.; Reibold, M.; Müller, J.; Paufler, P.; Meyer, D.C. Oriented growth of Sr_{n+1}Ti_nO_{3n+1} Ruddlesden–Popper phases in chemical solution deposited thin films. *J. Solid State Chem.* **2006**, *179*, 1864–1869. [[CrossRef](#)]
68. Haeni, J.H.; Irvin, P.; Chang, W.; Uecker, R.; Reiche, P.; Li, Y.L.; Choudhury, S.; Tian, W.; Hawley, M.E.; Craigo, B.; et al. Room-temperature ferroelectricity in strained SrTiO₃. *Nature* **2004**, *430*, 758–761. [[CrossRef](#)]
69. Perdew, J.P. Density functional theory and the band gap problem. *Int. J. Quantum Chem.* **1985**, *28*, 497–523. [[CrossRef](#)]
70. Riedl, T.; Gemming, T.; Weissbach, T.; Seifert, G.; Gutmann, E.; Zschornak, M.; Meyer, D.; Gemming, S. ELNES study of chemical solution deposited SrO(SrTiO₃)_n Ruddlesden–Popper films: Experiment and simulation. *Ultramicroscopy* **2009**, *1100*, 26–32. [[CrossRef](#)]
71. Zschornak, M.; Richter, C.; Nentwich, M.; Stöcker, H.; Gemming, S.; Meyer, D.C. Probing a crystal’s short-range structure and local orbitals by Resonant X-ray Diffraction methods. *Cryst. Res. Technol.* **2014**, *49*, 43–54. [[CrossRef](#)]
72. Stöcker, H.; Zschornak, M.; Richter, C.; Hanzig, J.; Hanzig, F.; Hinze, A.; Potzger, K.; Gemming, S.; Meyer, D.C. Surface-near modifications of SrTiO₃ local symmetry due to nitrogen implantation investigated by grazing incidence XANES. *Scr. Mater.* **2014**, *86*, 1–4. [[CrossRef](#)]